Model and simulations of the effects of polyelectrolyte coated electrodes in Capacitive Deionization

J.A. Lirio Piñar
Departamento de Física Aplicada, Facultad de Ciencias,
Universidad de Granada, 18071 Granada, Spain

J. Calvo
Departamento de Matemática Aplicada, Facultad de Ciencias,
Universidad de Granada, 18071 Granada, Spain and
Modeling Nature (MNat) Research Unit, University of Granada, Spain

S. Ahualli*
Departamento de Física Aplicada, Facultad de Ciencias,
Universidad de Granada, 18071 Granada, Spain and
Modeling Nature (MNat) Research Unit, University of Granada, Spain

(Dated: February 19, 2025)

The problem of ion transport in porous media is fundamental to many practical applications such as Capacitive Deionization, where ions are electrostatically attracted to a porous electrode and stored in the Electric Double Layer, leaving a partially desalinated solution. These electrodes are functionalized to achieve maximum efficiency: it is intended that for each depleted electron one ion is removed. For this purpose, the surface is coated with a polyelectrolyte layer of the same sign as the electronic charge. In this work, the movement of ions from the solution to the soft or polyelectrolyte-coated electrodes is studied. For this purpose, a 1-dimensional model is used to study the electric and diffusive fluxes produced by the application of an electric field and the storage of these ions in the micropores. The partial differential equations governing the process are numerically solved using the explicit Euler method. The results of the model indicate that the number of ions removed using soft electrodes is approximately 15 % greater than that achieved with bare electrodes. Ion adsorption kinetics show that coated electrodes provide slightly slower adsorption compared to bare electrodes. Regarding the charging time of the micropores, it can be seen that it is a faster process (characteristic time of 100 seconds) compared to the time in which the ion concentration reaches equilibrium: electromigration is faster than diffusion. Comparing the situations with and without polyelectrolyte coating, it is observed that saturation in the micropores is reached earlier when the electrodes are coated. Concerning the cell geometry, it has been found that the characteristic time is proportional to the length of the spacer and inversely proportional to the length of the electrodes. With regard to microporosity, the rate of the process is approximately constant, irrespective of the number of micropores. Moreover, the number of adsorbed ions strongly depends on their initial concentration. Finally, the analysis of the ionic diffusion coefficient is determinant in the kinetics of the process: taking into account the tortuosity of the porous electrode, which directly affects the diffusion in the channel, is fundamental to obtain model predictions close to reality.

I. INTRODUCTION

Capacitive Deionization (CDI) is considered one of the most attractive charge transfer process-based techniques for next-generation water treatment and purification. It has become a focus of attention in several studies [1–4] since 1990s due to the great possibilities of CDI to turn brackish water into fresh water by using small amounts of energy and its ionic separation capacity. In the last 10 years, there has been great progress thanks to the development of new materials and methods and the existence of advanced theoretical models that suggest ways for improvement. The key to the method lies in the capacitive property of the solid-liquid interface (typically porous carbon)/ionic solution. It is based on a simple and well-founded procedure from the physical point of view: it is sufficient to apply a small potential difference to a pair of porous electrodes so that many of the species present are removed from an ionic solution, due to the electrostatic attraction towards the corresponding electrode.

To understand the basis of CDI, let us imagine a pair of electrodes immersed in an electrolyte solution, and to which a potential difference (typically around 1 V to avoid water electrolysis) is applied externally. The pores of the electrodes acquire electronic charge, and thus an Electric Double Layer (EDL) will form that shields the surface charge. Ions removed from the solution and incorporated into the EDL render the solution, therefore, partially deionized or desalinated. It can then be said that capacitive desalination of the solution has been generated. This effect is encouraged by the extremely large

---

* Corresponding author
sahualli@ugr.es

surface area of the carbon electrodes. Because of its porous characteristics, 1 g of carbon can have a surface area of around 1500 m^2. Nevertheless, some studies show that only 10% of this surface is employed in the storage of ions [5]. The distribution of pores and the accessibility of these pores appear to be of significant importance in determining the efficiency of ion adsorption [6]. For this reason, we have proposed to study the transport of ions to the porous electrode and the physical phenomena that support it.

A number of studies attempt to achieve two main goals. On the one hand, innovative models are being developed to explain the dynamics of ions in CDI cells. This is a difficult aim because of the differences between the size scales of the electrodes (mm), macropores (μm), and micropores (nm) [7, 8]. Apart from that, many researchers have proposed modified methods to improve the efficiency of the CDI process. These upgrades involve the use of ionic exchange membranes [9, 10], new materials for electrodes [11], including ordered mesoporous carbon [12, 13], complex geometries for cells [14–16], putting aside the traditional flow-between architecture, or even using movable electrodes [17].

Ion adsorption occurs at the interface between the charged solid and the surrounding dilution. In other words, the ions are removed from the solution when the electrical double layer is built on the carbon porous surface. Indeed, the counterions are attracted to the surface, while the coions are repelled, resulting in an increase in the concentration of the former and a decrease in the latter. At low charge (low surface potential) the amount of ions attracted is comparable with the amount of those repelled. In this case, the ionic solution will not be desalinated. However, at higher surface potentials, coion concentration nearly drops to zero and more counterions are attracted to compensate for the surface charge, resulting in an asymmetry of both ion distributions. Therefore, there is a net adsorption of the salt in the dilution and hence desalination takes place. The phenomenon is reversed at the negative electrode, where a net electrical charge of a different sign is stored. The use of ion exchange membranes or polyelectrolyte coating is a common feature of the capacitive deionization. They block the expulsion of coions, and enhance the counterion entrance in such away that the counterions concentration increases comparing to the case of bare electrodes and therefore the efficiency of the systems.

These polyelectrolyte coated electrodes are called Soft Electrodes. Unfortunately, there have not been many theoretical studies on the effects of ionic transport using soft layers. However, previous results [18–22] seem to indicate that soft electrodes are highly effective in the CDI process when compared to bare electrodes. There are even fewer studies that propose models describing the dynamics in CDI cells that use soft electrodes.

This is the starting point for this work, whose objectives are to provide a theoretical description of the dynamics of the ions inside the cell and the polyelectrolyte coated pores, to solve the proposed equations with numerical methods, and to find the main parameters that optimize the CDI process.

II. THEORY

In order to predict the dynamic response of the system, the macroscopic cell architecture is reduced to a 1-dimensional model (Figure 1a). It comprises two porous electrodes separated by a spacer filled with a solution of two monovalent ionic species. The length of each of the electrodes is denoted as l_e, and l_s denotes the spacer length.

Nevertheless, the microscopic structure within the electrodes is complex because of the presence of multiple pore scales. First, carbon is full of pores ranging in size between 50 nm and 1 μm, known as "macropores". Furthermore, the material contains "micropores", which are approximately 1 nm in size. Figure 1b provides a schematic representation of this structure. These micropores can be considered as the regions where the EDL is formed, and a volumetric charge density caused by excess counterions can be found. As a counterpart, the spacer and macropores are large enough to avoid surface effects, thus maintaining electroneutrality.

The microscopic geometry of the electrodes can be summarized using two parameters: macroporosity p_{mA}, and microporosity p_{mi}. These parameters represent the volumes of the macropores and micropores, respectively, divided by the total volume of the electrodes. Consequently, their values are between zero and one, and their sum must be less than one. It should be noted that the spacer is entirely occupied by macropores ($p_{\mathrm{mA}} = 1$), and therefore, there are no micropores present ($p_{\mathrm{mi}} = 0$). With these considerations, the equations below are valid in any region of space, both electrodes and spacer.

Simplifications are required regarding the EDL, which can be achieved by introducing the modified Donnan model (mD model). This model assumes that the EDLs overlap inside the micropores as the thickness of the micropores is typically 2-3 nm for ionic concentrations of 10 mM or 20 mM of sodium chloride, NaCl, while the size of the micropore is around 1 nm. Therefore, the potential inside the micropores is assumed to be constant and equal to $\Delta\varphi_D$ (Donnan potential). These considerations allow us to decompose the potential, φ, at any position within the liquid phase in the cell as

$$\varphi = V_{app} - (\Delta\varphi_D + \Delta\varphi_{st})\, V_T. \qquad (1)$$

In equation (1), $\Delta\varphi_{st}$ represents the non-dimensional potential drop across the Stern layer and $\Delta\varphi_D$ is the potential difference between micropores and macropores. $V_T = e/k_B T$ is the thermal voltage, being k_B the Boltzmann constant, e the electron charge and T the temperature.

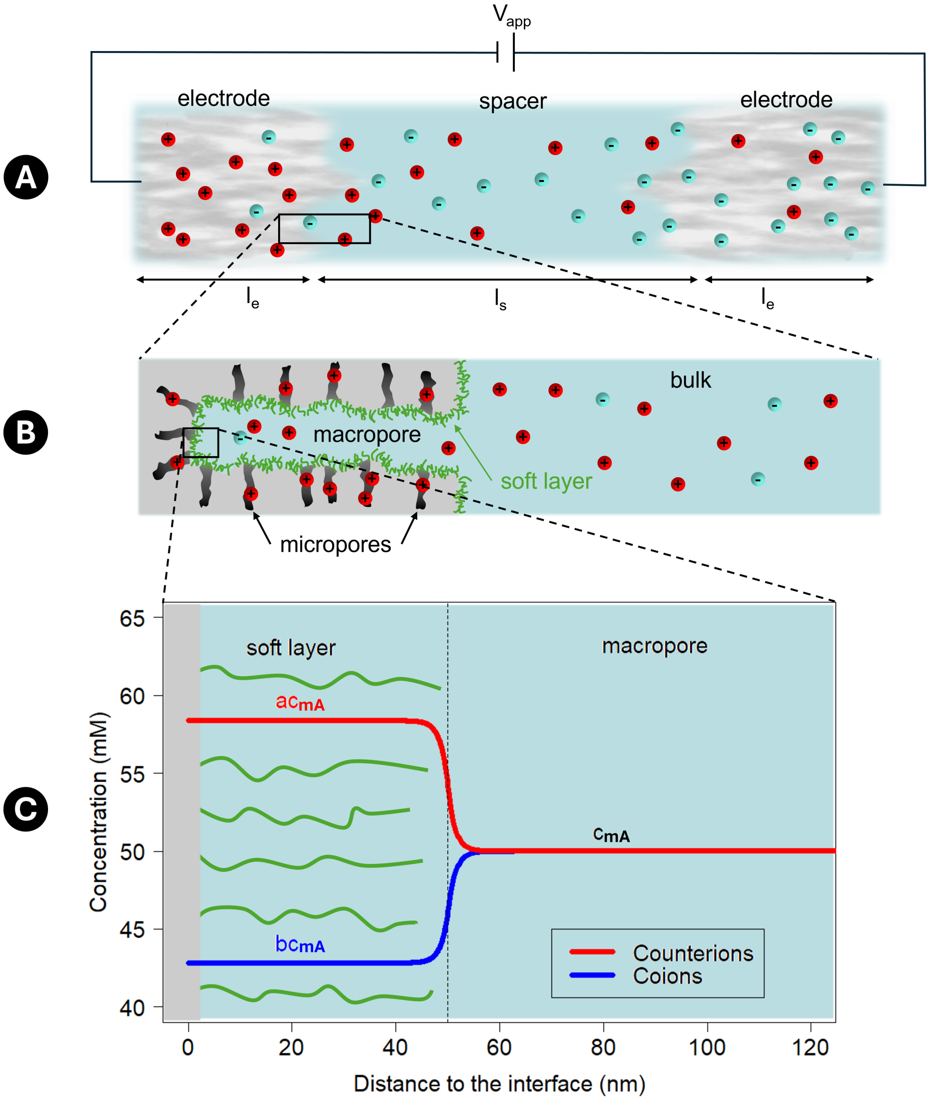

FIG. 1: Multiscale scheme of the CDI cell used for the model and simulation results of this study. (a) The cell consists of two carbon porous electrodes, each with a length of l_e, separated by a spacer of length l_s. The applied voltage is denoted as V_{app}. The height of the cell is not taken into account. (b) The porous structure of the carbon is made up of macropores, with a diameter between 50 nm and a few micrometers, and micropores, with a diameter of approximately 2 nm. The electrode surface, including that of the macropores, can be coated with a charged polyelectrolyte layer (green). (c) Within this layer, the concentration can be simulated by assuming a 50-nanometer-wide polyelectrolyte coating, obtaining a distribution that can be approximated to a Heaviside function: the counterion concentration remains constant and increases compared to the concentration in the bulk of the macropore. The opposite is true for coions.

A. Polyelectrolyte layer model

It is assumed that the polyelectrolyte layer is lining the walls of the macropores. As a result, ions are required to pass through this layer when moving from macro to micropores (as shown in Figure 1b). This layer facilitates the passage of counterions into the micropores while preventing the outflow of coions from the micropores into the solution when the Electrical Double Layer is formed. This ensures that, for each deposited charge on the surface of the electrode, one counterion will be removed from the solution, increasing the process efficiency to its ideal value of 1. The polyelectrolyte, whose polymer chains have charged repeating units, is permeable to the fluids and to the ions. However, in order to maintain electric neutrality due to the charged monomer groups, ions with opposite charges will be distributed in the region occupied by the polymer chains. Therefore, it is possible to conceive a model for the polyelectrolyte coating layer as a uniformly charged volumetric region with a charge density ρ_{pol}, which is permeable to ion flux. This region is known as the soft layer. To obtain the electric potential, φ, and ion concentration, c, close to the soft layer, the Poisson equation must be solved. Nevertheless, it must be split into two regions, inside the polyelectrolyte and beyond:

$$\begin{cases} \nabla^2\phi = -\frac{1}{\varepsilon\varepsilon_0}\rho_{sol} & \text{outside the soft layer,} \\ \nabla^2\phi = -\frac{1}{\varepsilon\varepsilon_0}(\rho_{sol}+\rho_{pol}) & \text{inside the soft layer,} \end{cases} \tag{2}$$

where the solution charge density, ρ_{sol}, coming from the accumulation or depletion of ions, is given by

$$\rho_{sol} = F(z_1 c_{1,\mathrm{mA}} + z_2 c_{2,\mathrm{mA}})\,. \tag{3}$$

Here we assume a binary electrolyte, so that $k = 1,2$ represents counterions and coions in solution, respectively. Although the scope of this paper is limited to binary, symmetric and monovalent electrolytes, at this stage we shall present the model in a way that it allows for any number of ionic species, as this might be useful elsewhere. In that way, z_k is the elemental charge of the ion type k and $c_{k,\mathrm{mA}}$ is the concentration in macropores. F stands for the Faraday constant.

A BVP4C MATLAB routine was developed to solve equations (2) and (3) considering a Boltzmann distribution for the ions in the soft layer with appropriate boundary conditions. Figure 1(c) shows the results for a given KCl concentration (50 mM) bathing a region coated with a soft layer.

It should be noted that the concentration of coions and counterions within the soft region, c_k^{SOFT}, remain relatively constant as long as the thickness of the polyelectrolyte layer is greater than that of the EDL. Consequently, to simplify the calculations, these amounts can be expressed as a multiple of the equilibrium concentration, c_{mA}:

$$c_1^{\mathrm{SOFT}} = a c_{\mathrm{mA}},\; c_2^{\mathrm{SOFT}} = b c_{\mathrm{mA}}. \tag{4}$$

In the previous relation, c_1^{SOFT} and c_2^{SOFT} are the concentrations of counterions and coions, respectively. Therefore, it is necessary that $a \geq 1$ and $0 < b \leq 1$.

B. 1D Model for the ionic transport

The starting point is the general form of the mass transport equation for an ion [23]:

$$\frac{\partial c_{k,\mathrm{total}}}{\partial t} = -\nabla\cdot\mathbf{j_k}.$$

In this model, both electric and diffusive terms contribute to the ionic flow. We use the conservation of ionic species during ion transport between micropores and macropores. Then we get

$$p_{\mathrm{mA}}\frac{\partial c_{k,\mathrm{mA}}}{\partial t} + p_{\mathrm{mi}}\frac{\partial c_{k,\mathrm{mi}}}{\partial t} = z_k\frac{\partial}{\partial x}\left(D_k p_{\mathrm{mA}} c_k^{\mathrm{SOFT}}\frac{\partial\tilde{\varphi}}{\partial x}\right) + \frac{\partial}{\partial x}\left(D_k p_{\mathrm{mA}}\frac{\partial c_{k,\mathrm{mA}}}{\partial x}\right), \tag{5}$$

where we recall that $k = 1,2$ represents counterions and coions in solution respectively, D_k is the diffusion coefficient, z_k is the elemental charge of the ion, $c_{k,\mathrm{mi}}$ is the concentration in micropores and c_k is the concentration in macropores. Furthermore, $\tilde{\varphi}$ is the non-dimensional potential associated with the one in the equation (1)

$$\tilde{\varphi} = \frac{\varphi}{V_T} = \frac{e\varphi}{k_B T}. \tag{6}$$

In the sequel a symmetric and monovalent electrolyte will be considered. What this means is that $k = 1,2$, and $z_1 = 1$, $z_2 = -1$ and D_1 is equal to D_2. One example of this kind of electrolyte is potassium chloride, KCl, where $D_K = 1.96010^{-9}\ m^2/s$ and $D_{Cl} = 2.03010^{-9}\ m^2/s$ [24].

Finally, as mentioned above, the macropores and the spacer are large enough to consider an electronneutrality situation. Thus, we set $c := c_{1,\mathrm{mA}} = c_{2,\mathrm{mA}}$. Then, using (4), the pair of equations (5) can be reduced to

$$p_{\mathrm{mA}}\frac{\partial c}{\partial t} + p_{\mathrm{mi}}\frac{\partial c_{1,\mathrm{mi}}}{\partial t} = D p_{\mathrm{mA}}\frac{\partial}{\partial x}\left(ac\frac{\partial\tilde{\varphi}}{\partial x} + \frac{\partial c}{\partial x}\right), \tag{7}$$

$$p_{\mathrm{mA}}\frac{\partial c}{\partial t} + p_{\mathrm{mi}}\frac{\partial c_{2,\mathrm{mi}}}{\partial t} = -D p_{\mathrm{mA}}\frac{\partial}{\partial x}\left(bc\frac{\partial\tilde{\varphi}}{\partial x} - \frac{\partial c}{\partial x}\right). \tag{8}$$

By adding and subtracting equations (7) and (8), we get to

$$2p_{\mathrm{mA}}\frac{\partial c}{\partial t} + p_{\mathrm{mi}}\frac{\partial\left(c_{1,\mathrm{mi}} + c_{2,\mathrm{mi}}\right)}{\partial t} = = D p_{\mathrm{mA}}\frac{\partial}{\partial x}\left[(a-b)c\frac{\partial\tilde{\varphi}}{\partial x} + 2\frac{\partial c}{\partial x}\right], \tag{9}$$

$$p_{\mathrm{mi}}\frac{\partial\left(c_{1,\mathrm{mi}} - c_{2,\mathrm{mi}}\right)}{\partial t} = (a+b) D p_{\mathrm{mA}}\frac{\partial}{\partial x}\left(c\frac{\partial\tilde{\varphi}}{\partial x}\right). \tag{10}$$

The term $\sigma_{\mathrm{mi}} := c_{1,\mathrm{mi}} - c_{2,\mathrm{mi}}$ multiplied by the Faraday constant F represents the charge density accumulated in micropores. Let us ellaborate on the expression $c_{1,\mathrm{mi}} + c_{2,\mathrm{mi}}$. Assuming equilibrium between micropores and macropores, the following relation can be proposed for their concentrations:

$$c_{k,\mathrm{mi}} = c\exp\left(-z_k\Delta\varphi_D + \mu_{k,att}\right), \tag{11}$$

where $\mu_{k,att}$ is a non-dimensional potential. This potential is introduced as an improvement to the modified Donnan model [3] over the basic one -see e.g. [9, 25, 26]. It represents the natural tendency of ions to enter micropores due to non-electrostatic interactions. These interactions involve both the electrode surface and the ions in the solution, being typically of chemical nature.

Furthermore, it is possible to establish a connection between the charge density and the capacitance of the Stern layer as follows:

$$\sigma_{\mathrm{mi}} = -\frac{C_{st,vol}\Delta\varphi_{st}V_T}{F}. \tag{12}$$

The equation includes the volumetric micropore Stern layer capacitance, denoted as $C_{st,vol}$.

Considering this, and remembering that the electrolyte is symmetric (thus $\mu := \mu_{1,att} = \mu_{2,att}$), the term $c_{1,\mathrm{mi}} + c_{2,\mathrm{mi}}$ will read

$$\begin{aligned} c_{1,\mathrm{mi}}+c_{2,\mathrm{mi}} &= 2ce^{\mu}\cosh\left(\Delta\varphi_D\right) = 2ce^{\mu}\sqrt{1+\sinh^2\left(\Delta\varphi_D\right)} \\ &= 2ce^{\mu}\sqrt{1+\left(\frac{\sigma_{\mathrm{mi}}}{2ce^{\mu}}\right)^2} = \sqrt{4c^2e^{2\mu}+\sigma_{\mathrm{mi}}^2}. \end{aligned} \tag{13}$$

Finally, the PDE system that describes the ion distribution in the CDI cell is

$$\begin{aligned} 2p_{\mathrm{mA}}\frac{\partial c}{\partial t} &+ p_{\mathrm{mi}}\frac{\partial\sqrt{4c^2e^{2\mu}+\sigma_{\mathrm{mi}}^2}}{\partial t} \\ &= Dp_{\mathrm{mA}}\frac{\partial}{\partial x}\left[(a-b)c\frac{\partial\tilde{\varphi}}{\partial x}+2\frac{\partial c}{\partial x}\right], \end{aligned} \tag{14}$$

$$p_{\mathrm{mi}}\frac{\partial\sigma_{\mathrm{mi}}}{\partial t} = (a+b)Dp_{\mathrm{mA}}\frac{\partial}{\partial x}\left(c\frac{\partial\tilde{\varphi}}{\partial x}\right), \tag{15}$$

$$\tilde{\varphi} = \frac{V_{app}}{V_T}+\operatorname{arcsinh}\left(\frac{\sigma_{\mathrm{mi}}}{2ce^{\mu}}\right)+\frac{F\sigma_{\mathrm{mi}}}{\left(C_{st,vol,0}+\alpha\sigma_{\mathrm{mi}}^2\right)V_T}, \tag{16}$$

where the unknowns are c, σ_{mi} and $\tilde{\varphi}$.

A charge-dependent Stern layer capacitance has been considered [3], expressed as $C_{st,vol} = C_{st,vol,0} + \alpha\sigma_{\mathrm{mi}}^2$ where $C_{st,vol,0}$ is the capacitance in the absence of charge, and α is a parameter which represents the deviation from the linear character of the Stern capacity when surfaces are charged.

The initial and boundary conditions for the concentration c, the charge density σ_{mi} and the non-dimensional potential $\tilde{\varphi}$ are given as follows (see Figure 2):

- The initial ion concentration must be uniform throughout the cell. Furthermore, there is zero charge density in micropores at $t = 0$,

$$c(x, t=0) = c_0, \qquad \sigma_{\mathrm{mi}}(x, t=0) = 0. \tag{17}$$

- The charge density is zero throughout the spacer as there are no micropores in this region.

- The potential at the electrode ends remains constant, with a value of $V_{app}/2V_T$ at the left (cathode) electrode end and $-V_{app}/2V_T$ at the right (anode) electrode end. Moreover, the electric potential in the spacer between the electrodes decays linearly, as no charge accumulates in this region.
- Ionic concentrations and electric potential must be continuous. As there is no net charge in the spacer, the potential decreases linearly from $\varphi\left(l_e^-\right)$ to $\varphi\left((l_e+l_s)^+\right)$.

- Since the electric and diffusive fluxes are zero at the ends of the cell, then

$$\frac{\partial c}{\partial x}(x=0,t) = \frac{\partial c}{\partial x}(x=l_s+2l_e,t) = 0, \tag{18}$$

$$\frac{\partial\tilde{\varphi}}{\partial x}(x=0,t) = \frac{\partial\tilde{\varphi}}{\partial x}(x=l_s+2l_e,t) = 0, \tag{19}$$

- The electric and diffusive fluxes must remain continuous across the interfaces that separate the electrodes and spacer region. As the available volumes for concentrations in the spacer and the electrodes differ, the fluxes must be multiplied by the porosity,

$$p_{\mathrm{mA}}\frac{\partial c}{\partial x}\left(x=l_e^-,t\right) = \frac{\partial c}{\partial x}\left(x=l_e^+,t\right), \tag{20}$$

$$p_{\mathrm{mA}}\frac{\partial\varphi}{\partial x}\left(x=l_e^-,t\right) = \frac{\partial\varphi}{\partial x}\left(x=l_e^+,t\right), \tag{21}$$

$$\frac{\partial c}{\partial x}\left(x=(l_e+l_s)^-,t\right) = p_{\mathrm{mA}}\frac{\partial c}{\partial x}\left(x=(l_e+l_s)^+,t\right), \tag{22}$$

$$\frac{\partial\varphi}{\partial x}\left(x=(l_e+l_s)^-,t\right) = p_{\mathrm{mA}}\frac{\partial\varphi}{\partial x}\left(x=(l_e+l_s)^+,t\right). \tag{23}$$

III. RESOLUTION METHOD

The finite difference method can be used to solve the previous PDE system. A time-marching scheme has been implemented using the explicit Euler method. Centered formulas are used to discretize spatial derivatives.

To implement the previous scheme, equation (14) must be rewritten accordingly. From equation (15), it follows

$$\frac{\partial\sigma_{\mathrm{mi}}}{\partial t} = (a+b)D\frac{p_{\mathrm{mA}}}{p_{\mathrm{mi}}}\frac{\partial}{\partial x}\left(c\frac{\partial\tilde{\varphi}}{\partial x}\right). \tag{24}$$

Therefore, the second term on the lhs of (14) can be expanded and then solved for the time derivative of c. In such a way, the following equation is obtained:

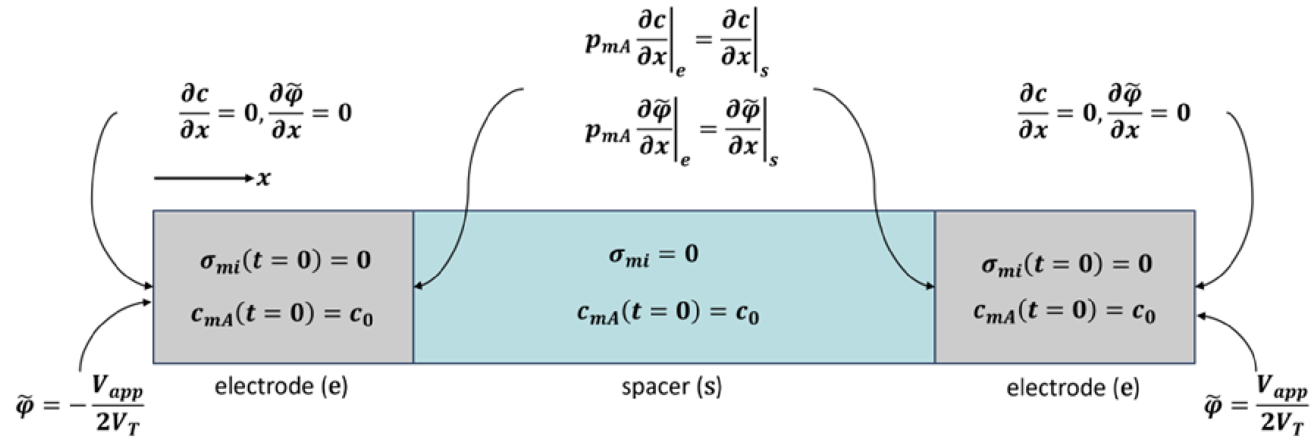

FIG. 2: Not to scale schematic of initial, boundary and interface conditions

$$\frac{\partial c}{\partial t} = \left(\frac{a-b}{2} D \frac{\partial}{\partial x}\left(c\frac{\partial \tilde{\varphi}}{\partial x}\right) + D\frac{\partial^2 c}{\partial x^2} - \frac{(a+b)D\sigma_{\mathrm{mi}}\frac{\partial}{\partial x}\left(c\frac{\partial\tilde{\varphi}}{\partial x}\right)}{4\sqrt{e^{2\mu}c^2 + \frac{\sigma_{\mathrm{mi}}^2}{4}}} \right) \times \left(1 + \frac{p_{\mathrm{mi}}e^{2\mu}c}{p_{\mathrm{mA}}\sqrt{e^{2\mu}c^2 + \frac{\sigma_{\mathrm{mi}}^2}{4}}} \right)^{-1} \tag{25}$$

This is complemented with equations (16) and (24). The flow diagram in Figure 3 represents the time-marching procedure.

To approximate the first derivatives with respect to the space variable in the first step of the numerical procedure, the centered difference formula is used,

$$\frac{\partial f}{\partial x}(a) \approx \frac{f(a+\Delta x) - f(a-\Delta x)}{2\Delta x}. \tag{26}$$

The exceptions are the endpoints of the cell, where $f(a+\Delta x)$ or $f(a-\Delta x)$ are undefined. In these cases, standard regressive or progressive difference formulas are used instead. Second spatial derivatives are approximated using the standard second-order centered difference formula.

The Explicit Euler method requires a time step parameter, Δt, and a spatial grid with intervals of length Δx, that divides the total length of the cell, $l_s + 2l_e$, in $N := 1 + (l_s + 2l_e)/\Delta x$ nodes (see in Figure 4).

Note that the simulation provides more accurate results with lower values of Δt and Δx. Furthermore, to avoid instabilities we have to operate the method under a constraint of the form $\Delta t = O((\Delta x)^2/(2D))$, see e.g. [27].

IV. RESULTS

A. Simulation parameters

This study examines the ion transport kinetics in a porous electrode and compares the performance of a polyelectrolyte-coated electrode with that of an uncoated electrode. To analyse how the main parameters affecting this problem impact transport, we have selected a set of standard experimental parameters for the simulations, as shown in Table I. The temporal and spatial responses of the system have been studied by varying some of these parameters.

Although increasing the layers of one electrode improves the overall adsorption of the system, it is optimal to use electrodes of the same size when considering adsorption per gram of electrode. This corresponds both to the modified Donnan model and to the experimental observations [28]. That is why the lengths of the anode and cathode are the same ($l_e = l_{anode} = l_{cathode}$) and electrodes of different lengths will not be considered.

Moreover, the diffusion coefficient will be taken approximately as that of potassium chloride, KCl, which, as mentioned above, is a binary, almost symmetric and monovalent electrolyte.

It is assumed that the simulations run under the parameters given in Table I by default, unless otherwise stated.

B. Correction factors depending on the polyelectrolyte charge

The parameters mentioned above are dependent on the physical properties of the system. In addition to these parameters, the values of factors a and b are also required. These values are associated with the volumetric charge of the polyelectrolyte coating and the solution concentration in which they are immersed. Specifically, they can be calculated as ratios of concentrations inside and outside the soft layer, see (4). The MATLAB routine

TABLE I: Set of standard parameters used in the simulations. The last three parameters have been taken from [3].

Magnitude	Value
Thickness of the spacer (spacer length)	$l_s = 1$ mm
Thickness of the electrodes (electrode length)	$l_e = 0.5$ mm
Spatial step	$\Delta x = 0.01$ mm
Total time	$t_{max} = 500$ s
Time step	$\Delta t = 0.001$ s
Applied voltage	$V_{app} = 1$ V
Temperature	$T = 300$ K
Initial ionic concentration	$c_0 = 50$ mM
Macroporosity	$p_{\text{mA}} = 0.5$
Microporosity	$p_{\text{mi}} = 0.2$
Ion diffusion coefficient	$D = 2 \times 10^{-9}$ m^2/s
Non-dimensional potential μ	$\mu = 1.4$
Volumetric capacitance of Stern layer without charged	$C_{st,vol,0} = 1.2 \times 10^9$ F/m^3
Parameter α	$\alpha = 17$ F·m^3/mol^2

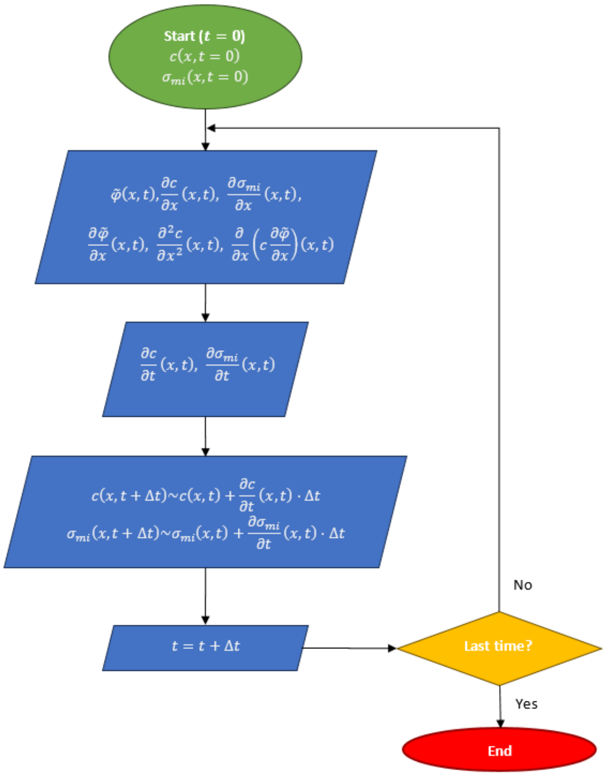

FIG. 3: Flow chart of the Explicit Euler method used for the calculation of the evolution of concentrations and charges. It is based on the approximation given by $f'(x) \approx (f(x+h) - f(h))/h$.

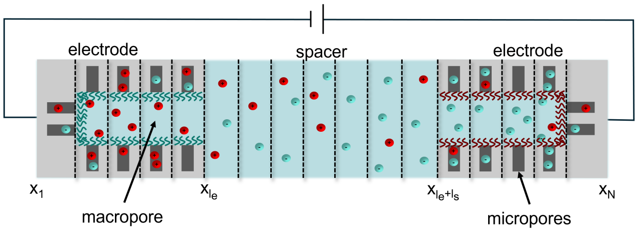

FIG. 4: Scheme of a cell divided into N nodes. Electrode walls are represented in grey, micropores in black, and both the spacer (in the center) and macropores (in the electrode area) in blue. The indices of the anode nodes vary between x_1 and x_{l_e}, those of the spacer between x_{l_e} and $x_{l_e+l_s}$, and those of the cathode between $x_{l_e+l_s}$ and x_N.

mentioned above returns the values of a and b as a function of polyelectrolyte charge density, ρ_{pol}, as shown in Figure 5.

It can be seen that highly charged polyelectrolytes and low concentrated solutions have a greater impact on coion and counterion concentrations. Additionally, the value of a increases exponentially with the charge, while the value of b appears to have a lower limit that cannot be lower than zero.

C. Comparison between simulation with and without soft layer

This section will analyse the effect of polyelectrolyte coating by comparing the concentration distribution over time. To achieve this, we will take the values of the polyelectrolyte charge density from previous experimental results [18]. The outputs of the simulations are visible in Figure 6a. Note that the qualitative behaviour aligns with the predictions made by other authors in the studied region (spacer) [26].

Figure 6a shows that the concentration decreases most rapidly at the boundary between the electrode and the spacer (x_{50}). This is because the concentration is initially constant throughout the entire cell. Thus its spatial derivative is zero. The potential is constant along the electrodes with value $V_{app}/2V_T$ on the left and $-V_{app}/2V_T$ on the right, and decays linearly be-

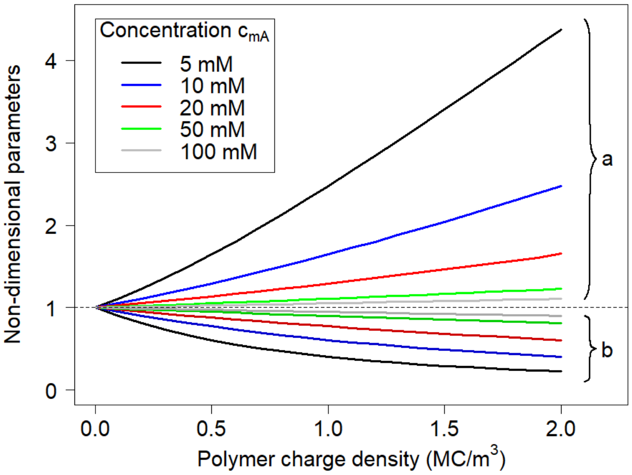

FIG. 5: Simulated values for parameters a (greater than 1) and b (less than 1) for typical polyelectrolyte charge and solution concentration values.

tween those two values in the spacer. Therefore, the second derivative of the potential with respect to x is nonzero only at the boundary between the electrode and the spacer. This causes the time derivative of the concentration to be non-zero at this point, where the concentration begins to decrease. As time advances, the concentration diffuses in and out of the electrode.

On the other hand, the innermost point of the electrode (x_2) experiences the greatest decrease in concentration. This is because an ion must pass through the entire electrode to reach this point by diffusion from the spacer, making it more likely to be adsorbed before arriving.

As can be seen in Figure 6a, concentrations at different points equalize over time. This happens when the double layer reaches equilibrium and enough ions have been adsorbed to shield the charge of the electrode (and the polyelectrolyte, if present). At this time, the potential difference across the cell becomes zero, cancelling the electric flow of ions. Then those begin to redistribute by diffusion until they reach an equilibrium concentration throughout the space.

The predictions for polyelectrolyte coated electrodes follow the same trend but the final concentration at equilibrium is reduced, indicating that ion extraction is more efficient. The predictions of the model demonstrate an increase of 18.34% in the number of ions removed with the use of a polyelectrolyte coating.

However, adsorption process in both cases have similar characteristic times. An adjusted exponential model is used,

$$c(t) = A \exp\left(-\frac{t}{\tau}\right) + c_\infty, \tag{27}$$

where A is a multiplicative constant, τ is the characteristic time of the CDI process, and c_∞ is the limit concentration to infinite time. By fitting the time evolution of the concentration in the spacer (x_{100}), the characteristic time is 90.4 s and 94.0 s without and with polyelectrolyte coating respectively, giving a slight difference in the kinetics of the process; therefore, the coating brings a slower adsorption. The spatiotemporal surface generated by the solution in every point of the spacer at every time instant can be seen in Figure 7 (A).

It is important to note that the reduction in the number of ions is significantly greater than that observed in an experimental setting involving a real CDI cell. This is due to the fact that we are utilising a simplified one-dimensional model, which is more analogous to a section of a real cell without convection.

The charge accumulated inside micropores (not present at the spacer) can also be analyzed, as shown in Figure 6b. It has been represented just for the first 100 seconds because for longer times evolution curves almost overlap. The same occurs for the potential. Thus, after this time, there is hardly any dynamics, in agreement with the observations from the time evolution of ionic concentration: the electromigration is faster than the diffusion.

The point at which the adsorption of charge occurs faster is at the border between the electrode and the spacer (x_{50}) because the time derivative of σ_{mi} depends on the second spatial derivative of the potential, see (24). At every point inside the electrode the accumulated charge increases (in absolute value) until it reaches a saturation level, which is around 70.77 MC/m^3. This occurs when the electrical double layer in the micropores has already accumulated enough counterions to shield the electrode charge and is, therefore, independent of the polyelectrolyte charge (located in macropores).

Comparing the situations with and without polyelectrolyte coating, it is possible to observe that the saturation in the micropores is reached earlier when the electrodes are coated. Moreover, the final adsorbed charge is slightly higher in the latter case: Figure 7 (C) shows a difference of about -3.95 mM when we use a polyelectrolyte coating with electrical charge 1 MC/m^3 with respect to when there is no polyelectrolyte coating in the spacer after 500 s. The determining factor for the increase in efficiency due to the coating is due to the first term of the second member of equation (10), which comes from an enhancement of the counterion flow into the micropores and the blocking of the coion flow. The figure also shows that the most significant changes take place in the initial instants (before 100 seconds). This is due to the influence of the polyelectrolyte layer on the electric flux, which is dominant at these times: the presence of the soft layer facilitates the rapid migration of counterions towards the electrodes at the initial stages of the CDI process.

The detailed work on the charge dynamics of porous electrodes, conducted by Lian et al. [29] demonstrates that the electrode charge process can be divided into two distinct time scales. One is associated to the formation of double layer, which can be conceptualised as a capacitor with a characteristic time of $\kappa^{-1} l_s / 2D$, where κ is

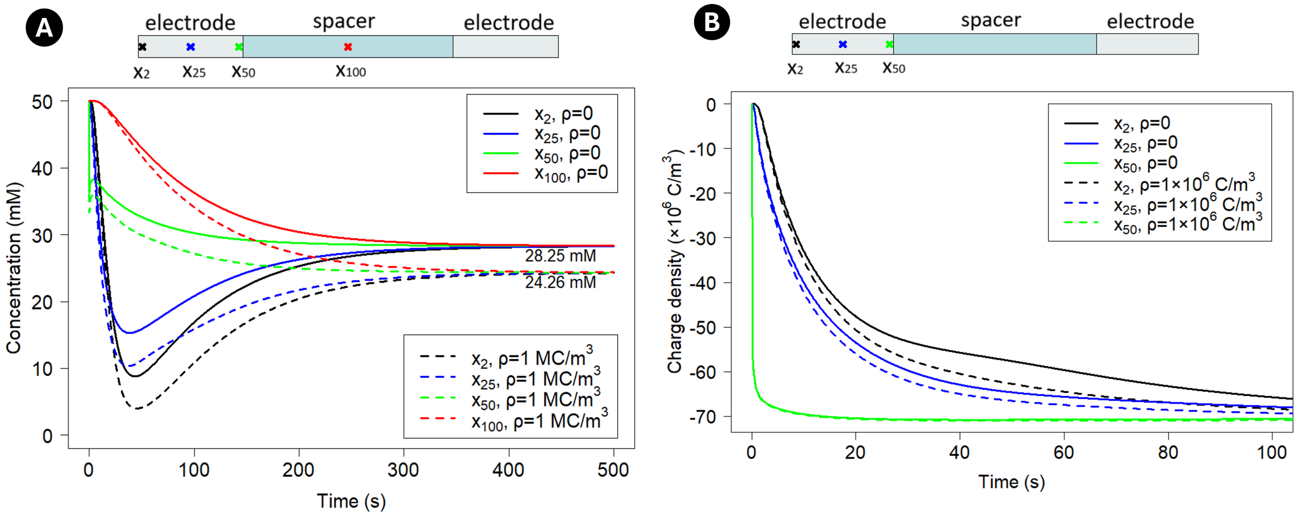

FIG. 6: (a) Concentration of ions in the macropores over 500 seconds of time. Solid lines represent a cell without polyelectrolyte coating, while dotted lines represent a charge density $\rho = 1$ MC/m^3. The concentration is represented at the end of the electrode (x_2, black), at its midpoint (x_{25}, blue), at the interface between the electrode and the spacer (x_{50}, green), and at the midpoint of the spacer (x_{100}, red). (b) Charge accummulated in micropores, here shown at x_2, x_{25} and x_{50} and only over the first 100 seconds.

the inverse of the Debye length. However, in the context of a porous electrode, a set of n parallel electrodes (transmission line model) is considered, resulting in a longer generalised relaxation time in comparison to RC. The other mechanism is associated with the transport of salt across the electrode, which arises from the accumulation of charge in the micropores. The time scale for this mechanism, as determined by Lian et al., is given by $(l_e + l_s/2)^2/D$. This value is 500 s for our system.

It is interesting to point out that, if the graphs representing the temporal evolution of the ion concentration in the macropores (Figure 6a) and the evolution of the accumulated charge in the micropores (Figure 6b) are compared, it is observed that the equilibrium concentration is reached at approximately 400 seconds, in good agreement with the previous calculated value (500 s), while the micropore charge reaches a stationary level at around 150 seconds. This behavior reveals that the shielding of the electrodes occurs first, which ceases the charge adsorption. From this moment on, there begins the redistribution of concentrations by diffusion in the absence of an electric field. The diffusion process is slower than electromigration and the ions are redistributed along the cell until they equalize their concentration throughout space.

Using the fit curve given by (27) to obtain the characteristic charge times (at the midpoint of the electrodes), we get 13.8 seconds and 16.2 seconds without and with charged polyelectrolyte respectively. If these values are compared with those obtained for the concentration in the spacer, we can conclude that the accumulation of charges in the pores is much faster than the decrease in concentration.

For this reason, the correct choice of porous material for the electrode is very important. Physical aspects that increase the diffusion time should be avoided if a fast adsorption of ions on the electrodes is wanted.

D. Length of electrodes and spacer

Other magnitudes of interest are the lengths of the electrodes and the spacer and their dependences with the adsorption dynamic. To analyze this relation, $r = l_s/l_e$ is defined as the ratio between the spacer and electrodes lengths.

In Figure 8 it can be seen how the concentration of ions evolves at the midpoint of the spacer when electrode and spacer have the same length ($r = 1$), double ($r = 2$) and quadruple ($r = 4$). As expected, the lower the ratio of spacer to electrode length, the greater the adsorption that occurs. This is because, for low values of r, there is more space available in micropores to store ions in relation to their total amount in the spacer. That is one of the reasons why, when a CDI process is carried out on a larger scale, the space between electrodes must be minimal to increase ion adsorption, even if then the dissolution flow between electrodes is lower.

The characteristic times of the different simulations are summarized in Table II. It can be observed that the characteristic time τ and the ratio of lengths r follow approximately a linear relationship,

$$\frac{r}{\tau} \propto k.$$

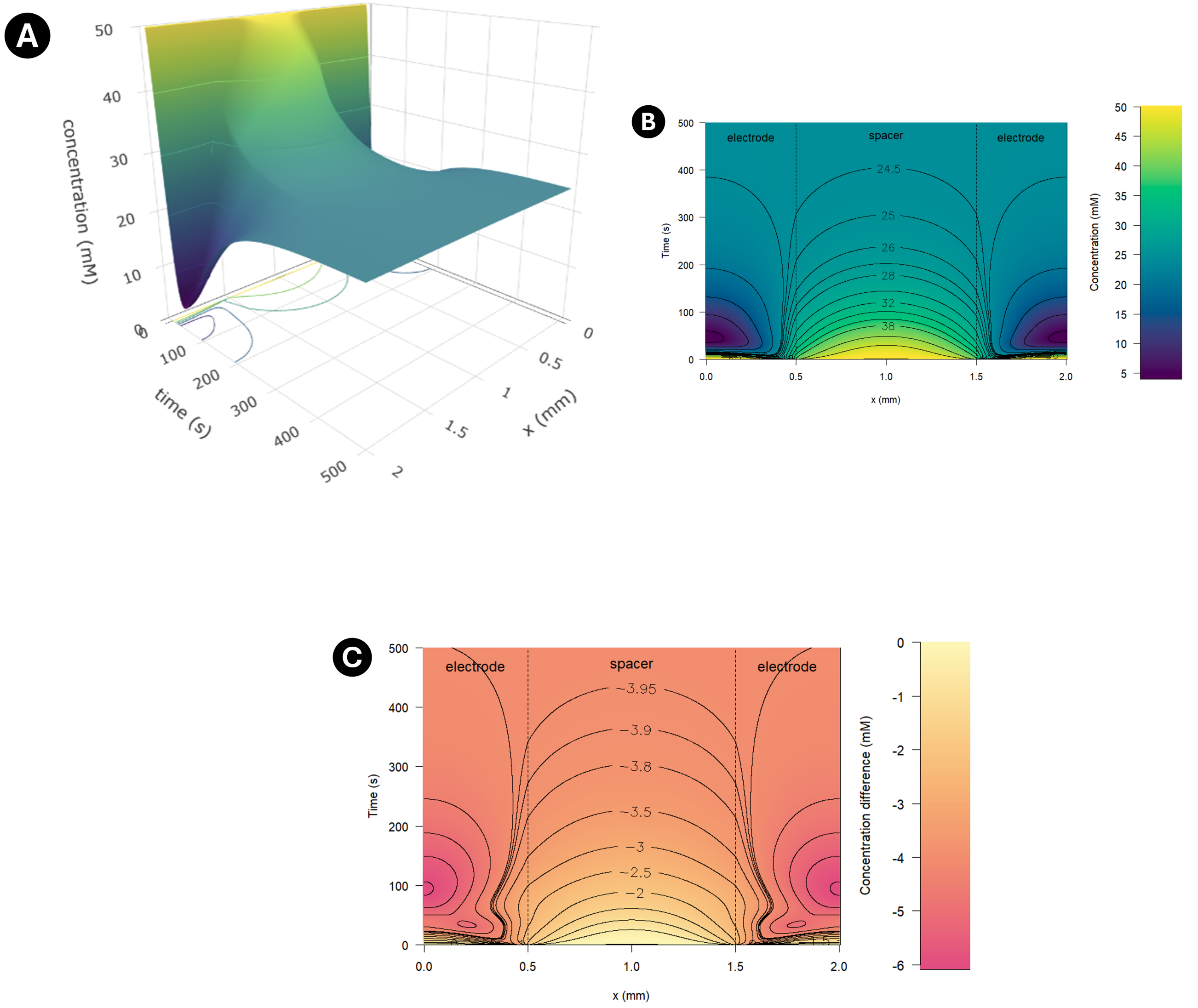

FIG. 7: Concentration surface as a function of spatial and temporal variables **(A)** an corresponding heat map (in mM) **(B)** when using a polyelectrolyte coating of with charge density $\rho = 1$ MC/m^3. The difference with respect to the case where no coating is used is represented by a heat map (in mM) **(C)**.

This is reasonable since capacitive deionization is a surface charge storage process. Therefore, the smaller the electrodes, the less surface area is available. Also, the larger the spacer, the longer it will take for the concentration to change from the surface of the electrodes to the center of the spacer. This causes the characteristic time to behave proportionally with l_s and inversely proportional to l_e.

TABLE II: Characteristic times for the curves in Figure 8 obtained from the fitting using Eq. (27).

Characteristic time τ (s)			
	$r = 1$	$r = 2$	$r = 4$
$\rho = 0$ MC/m^3	55.07 ± 0.02	90.41 ± 0.18	205.9 ± 1.4
$\rho = 0.5$ MC/m^3	56.53 ± 0.02	91.99 ± 0.18	208.6 ± 1.4
$\rho = 1$ MC/m^3	58.27 ± 0.03	94.04 ± 0.17	212.3 ± 1.5

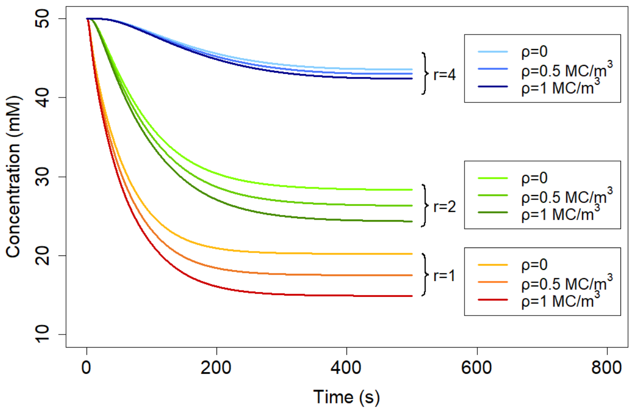

FIG. 8: Concentration of ions at the midpoint of the spacer (x_{100}) as a function of time. All simulations above have electrode lengths of $l_e = 0.5$ mm. Blue lines represent spacer length of $l_s = 2$ mm, green lines represent $l_s = 1$ mm, and orange lines represent $l_s = 0.5$ mm. Each color tone represents a charge value for the polyelectrolyte coating.

E. Microporosity

In equations (24) and (25) the parameters p_{mA} and p_{mi} just appear as the ratio $p = p_{\mathrm{mA}}/p_{\mathrm{mi}}$. Therefore, to explore how the system behaves in our simulations, we keep the macroporosity p_{mA} constant (as indicated in Table I) and vary the microporosity p_{mi} accordingly. The results can be seen in Figure 9.

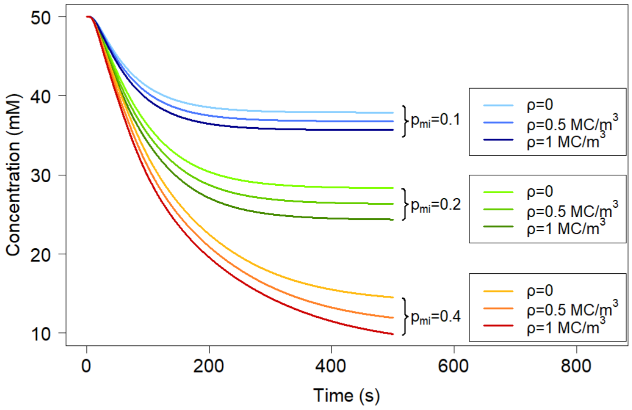

FIG. 9: Concentration of ions in the macropores over 500 seconds of time. Blue lines represent a cell whose electrodes have a microporosity $p_{\mathrm{mi}} = 0.1$, green lines represent $p_{\mathrm{mi}} = 0.2$, and orange lines represent $p_{\mathrm{mi}} = 0.4$.The concentration is represented at the midpoint of the spacer (x_{100}). Each color tone represents a charge value for the polyelectrolyte coating.

TABLE III: Characteristic times for the curves in Figure 9 obtained from fitting using Eq. (27).

Characteristic time τ (s)			
	$p_{\mathrm{mi}} = 0.1$	$p_{\mathrm{mi}} = 0.2$	$p_{\mathrm{mi}} = 0.4$
$\rho = 0$ MC/m^3	71.64 ± 0.14	90.41 ± 0.18	137.70 ± 0.16
$\rho = 0.5$ MC/m^3	71.76 ± 0.14	91.99 ± 0.18	140.37 ± 0.16
$\rho = 1$ MC/m^3	71.91 ± 0.14	94.04 ± 0.17	140.40 ± 0.18

As expected, the higher the microporosity value, the further the remaining ion concentration in the spacer decreases. This is because there is a greater volume available to store adsorbed ions.

The concentration of ions removed from the solution is increased from 13 mM with low porosity to approximately 36 mM using higher carbon porosity -depending on the charge density of the polyelectrolyte. This high value is explained by the large amount of free space available for ion removal, as indicated by $p_{\mathrm{mi}} = 0.4$ and $p_{\mathrm{mA}} = 0.5$, which means that it is 90% of the total volume. For example, values in [26] obtained by dry/water-saturated measurements of the electrode mass and N_2 adsorption porosimetry measurements are $p_{\mathrm{mi}} = 0.2$ and $p_{\mathrm{mA}} = 0.57$.

As we can see in Table III, the characteristic time increases substantially when the microporosity is increased. The characteristic time for carbon with a porosity ratio $p = 5$, which means a low microporosity, is 95% longer than that of those with $p = 1.25$, A very high value of microporosity compared to macroporosity. However, comparing the number of ions removed, and defining the velocity of the process as $c_{removed}/\tau$, it can be seen that the process speed is approximately the same regardless of microporosity (in the specific case of a coating with 0.5 MC/m^3 of electrical charge, the ion adsorption velocities are 0.184, 0.256 and 0.271, respectively, for p_{mi} values of 0.1, 0.2 and 0.4). The only noticeable difference is that a longer time is needed for high microporosity values since adsorption is higher.

F. Initial concentration

As Figure 10 indicates, the number of ions adsorbed in the process depends strongly on their initial concentration. To be able to compare the processes of CDI with different initial concentrations, the non-dimensionalized concentration c/c_0 is used.

For the standard concentration (50 mM) used in this work, the concentration drop is approximately 48% after the adsorption step. However, if the same process is performed with a less concentrated solution (20 mM) the drop increases substantially (94% of ions removed). This result confirms that the association of many cells is necessary to handle higher salt concentrations. If this is not feasible, then hybrid deionization systems are required for desalinating seawater (500 mM NaCl) since e.g. for a solution of 100 mM the number of ions removed is only

TABLE IV: Characteristic times for the curves in Figure 10 obtained from fitting using Eq. (27).

Characteristic time τ (s)			
	$c_0 = 20$ mM	$c_0 = 50$ mM	$c_0 = 100$ mM
$\rho = 0$ MC/m^3	112.86 ± 0.18	90.41 ± 0.18	85.25 ± 0.12
$\rho = 0.5$ MC/m^3	105.61 ± 0.17	91.99 ± 0.18	85.12 ± 0.12
$\rho = 1$ MC/m^3	100.15 ± 0.15	94.04 ± 0.17	85.00 ± 0.11

14%.

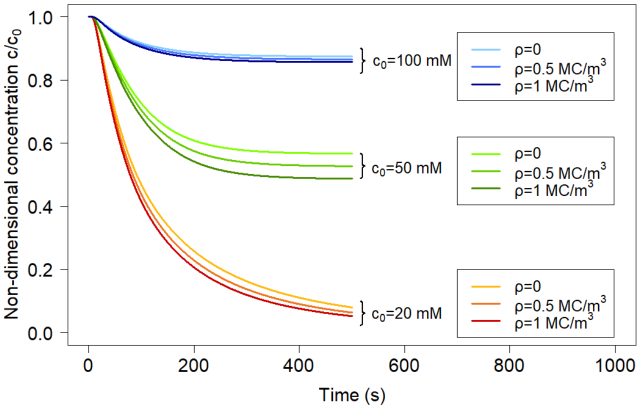

FIG. 10: Concentration of ions in the macropores over 500 seconds of time. Blue lines represent a cell with an initial concentration of $c_0 = 100$ mM; green lines represent $c_0 = 50$ mM and orange lines represent $c_0 = 20$ mM. The concentration is represented at the midpoint of the spacer (x_{100}). Each color tone represents a charge value for the polyelectrolyte coating.

About the characteristic times, Table IV shows that the effect of the initial concentration is less decisive than that produced by other parameters. Even so, the trend in the data is clear: lower concentrations slow down the process.

G. Ionic diffusion coefficients

Finally, the analysis of the diffusion coefficient of the ions involved in desalination is decisive in the kinetics of the process. This is not influenced by the quantity of ions removed, which depends solely on the formation of the electric double layer. This behavior can be observed in Figure 11a.

Changes in diffusion coefficients do not cause ion adsorption variations, as it is shown by the fact that the curves corresponding to the same polyelectrolyte charge values tend to the same final concentration at sufficiently long times. They do, however, affect the speed of stabilization of the CDI process. The characteristic times are set out in Table V.

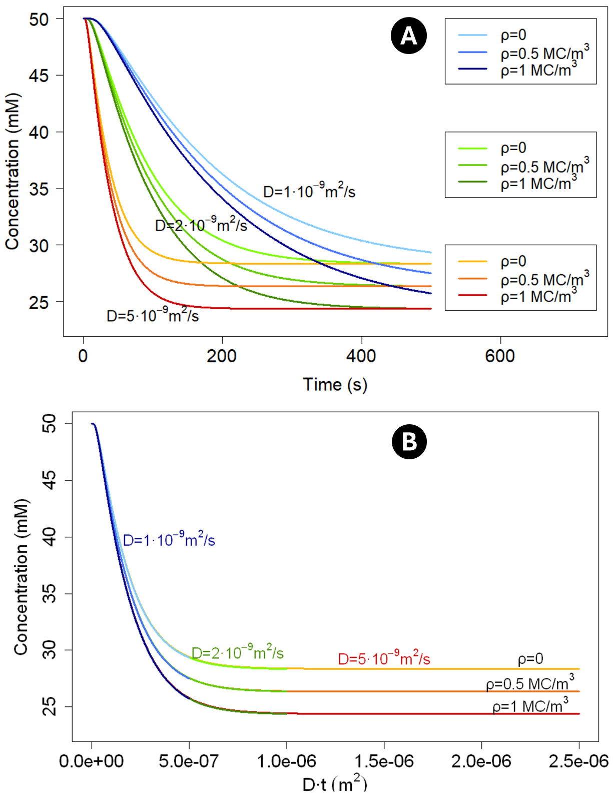

FIG. 11: Concentration of ions in the macropores as a function of (a) the time and (b) the product of the diffusion coefficient and the time, $D \cdot t$. Blue lines represent a cell whose ions have a diffusion coefficient of $D = 1 \times 10^{-9}$ m^2/s; green lines represent $D = 2 \times 10^{-9}$ m^2/s and orange lines represent $D = 5 \times 10^{-9}$ m^2/s. The concentration is represented at the midpoint of the spacer (x_{100}). Each color tone represents a charge value for the polyelectrolyte coating.

This phenomenon is also evident in Figure 11b, which illustrates that the concentration graphs as a function of the product $D \cdot t$ do overlap for identical polyelectrolyte charge values. The curves for the three diffusion coefficient are plotted from 0 to $D \cdot t_{max} = 0.5; 1.0; 2.5 \times 10^{-6}$ m^2 respectively, given that t_{max} is equal to 500 seconds and the value of D varies. Nevertheless, our findings indicate that the concentration evolution curves continue to overlap when simulations are extended to 1250 seconds for $D = 2 \times 10^{-9}$ m^2/s (green lines in Figure 11b) and 2500 seconds for $D = 1 \times 10^{-9}$ m^2/s (blue lines). This is consistent with the hypothesis that the value of D does not impact the adsorption dynamics of the ions, but rather influences the kinetics.

These differences in characteristic times are so significative that they may lead to the development of selective methods to remove only certain types of ions from a solution, while others remain in it, based on diffusion coefficient differences between those ions.

On the other hand, the ions inside the macropores do

TABLE V: Characteristic times for the curves in Figure 11a obtained from fitting Eq. 27. Diffusion coefficient D has $\times 10^{-9}\,\mathrm{m}^2/\mathrm{s}$ units.

Characteristic time τ (s)			
	$D = 1$	$D = 2$	$D = 5$
$\rho = 0\ \mathrm{MC/m^3}$	209.3 ± 0.7	90.41 ± 0.18	34.93 ± 0.06
$\rho = 0.5\ \mathrm{MC/m^3}$	212.5 ± 0.6	91.99 ± 0.18	35.51 ± 0.06
$\rho = 1\ \mathrm{MC/m^3}$	216.0 ± 0.6	94.04 ± 0.17	36.26 ± 0.06

not diffuse in the same way as those within the solution, which would lead us to think that a more appropriate model should take into account that the tortuosity of the macropores affects the adsorption kinetics.

V. CONCLUSIONS

In this work a simple 1D model has been proposed for the first time to explain the ion adsorption capacity and dynamics change when soft electrodes are used in Capacitive Deionization. By numerically solving the equations governing the process, it has been possible to analyze the dependence of ion removal and characteristic time of CDI process on parameters such as the diffusion coefficient, the length of electrodes and spacer, the initial electrolyte concentration, the carbon porosity and, of course, the charge of the polyelectrolyte coating.

In addition to providing a theoretical basis that explains the functioning of the soft layer in a simple way and effectively proving the positive implications of the addition of this layer, the consequences drawn are as expected and agree with those of other authors using bare electrodes. These findings indicate that ion adsorption increases with electrode thickness (or decreasing spacer width) and with microporosity. Furthermore, the amount of adsorbed ions is independent of the initial concentration, resulting in higher relative adsorption using lower concentrations. Finally, the diffusion coefficient of the extracted ions does not affect the amount of ions removed. However, shorter characteristic times occur when using ions with a higher diffusion coefficient.

In all simulations, it has been observed that the addition of a soft layer on the electrodes significantly increases the number of ions removed during the capacitive deionisation process, with an increase of approximately 15% by averaging all simulations carried out in this work. This is accompanied by a minimal impact on the characteristic time. This represents a remarkable improvement in the efficiency of the CDI cell for the desalination of highly saline water.

ACKNOWLEDGMENTS

Financial support of this investigation by the grant TED2021-131855BI00/AEI/10.13039/501100011033/Unión Europea Next Generation EU/PRTR is gratefully acknowledged.

J. C. has been partially supported by Grant C-EXP-265-UGR23 funded by Consejería de Universidad, Investigación e Innovación & ERDF/EU Andalusia Program, by Grant PID2022-137228OB-I00 funded by the Spanish Ministerio de Ciencia, Innovación y Universidades, MICIU/AEI/10.13039/501100011033 & "ERDF/EU A way of making Europe". J.C and S.A have been partially supported by Modeling Nature Research Unit, project QUAL21-011.

---

[1] J. Farmer, R. Pekala, D. Fix, J. Phillips, J. Poco, and C. Alviso, Capacitive deionization: New water treatment technology, Chemistry & Materials Science , 134.

[2] Y. Oren, Capacitive deionization (cdi) for desalination and water treatment—past, present and future (a review), Desalination **228**, 10 (2008).

[3] S. Porada, R. Zhao, A. van der Wal, V. Presser, and P. M. Biesheuvel, Review on the science and technology of water desalination by capacitive deionization, Progress in materials science **58**, 1388 (2013).

[4] M. A. Ahmed and S. Tewari, Capacitive deionization: Processes, materials and state of the technology, Journal of Electroanalytical Chemistry **813**, 178 (2018).

[5] A. Delgado, S. Ahualli, M. Fernández, M. González, G. Iglesias, J. Vivo-Vilches, and M. Jiménez, Geometrical properties of materials for energy production by salinity exchange, Environmental Chemistry **14**, 279 (2017).

[6] C. Liu, Q. Li, W. Kang, W. Lei, X. Wang, C. Lu, and M. Naebe, Structural design and mechanism analysis of hierarchical porous carbon fibers for advanced energy and environmental applications, Journal of Materials Chemistry A **10**, 10 (2022).

[7] R. Liu, S. Yao, and Y. Shen, Pore-scale investigation on ion transport and transfer resistance in charged porous media with micro-macro structure, Journal of Molecular Liquids **320**, 114481 (2020).

[8] R. Liu, L. Chen, S. Yao, and Y. Shen, Pore-scale study of capacitive charging and desalination process in porous electrodes and effects of porous structures, Journal of Molecular Liquids **332**, 115863 (2021).

[9] R. Zhao, O. Satpradit, H. Rijnaarts, P. Biesheuvel, and A. Van der Wal, Optimization of salt adsorption rate in membrane capacitive deionization, Water research **47**, 1941 (2013).

[10] G. Folaranmi, M. Bechelany, P. Sistat, M. Cretin, and F. Zaviska, Towards electrochemical water desalination techniques: a review on capacitive deionization, membrane capacitive deionization and flow capacitive deionization, Membranes **10**, 96 (2020).

[11] P. Srimuk, X. Su, J. Yoon, D. Aurbach, and V. Presser, Charge-transfer materials for electrochemical water desalination, ion separation and the recovery of elements, Nature Reviews Materials **5**, 517 (2020).

[12] Z. Peng, D. Zhang, L. Shi, and T. Yan, High performance

ordered mesoporous carbon/carbon nanotube composite electrodes for capacitive deionization, Journal of Materials chemistry **22**, 6603 (2012).

[13] S. Tian, J. Wu, X. Zhang, K. K. Ostrikov, and Z. Zhang, Capacitive deionization with nitrogen-doped highly ordered mesoporous carbon electrodes, Chemical Engineering Journal **380**, 122514 (2020).

[14] Z. Gu, B. Xu, P. Huo, S. M. Rubinstein, M. Z. Bazant, and D. Deng, Deionization shock driven by electroconvection in a circular channel, Physical Review Fluids **4**, 113701 (2019).

[15] T. Mubita, S. Porada, P. Biesheuvel, A. van der Wal, and J. Dykstra, Capacitive deionization with wire-shaped electrodes, Electrochimica acta **270**, 165 (2018).

[16] Z. Gu, B. Xu, P. Huo, M. Su, and D. Deng, Electroconvection instability and shocks in complex geometries, Current Opinion in Colloid & Interface Science **60**, 101604 (2022).

[17] K. Dermentzis and W. Wessner, Continuous capacitive deionization with regenerative rotating film electrodes, Electrochemistry Communications **92**, 5 (2018).

[18] S. Ahualli, G. R. Iglesias, M. M. Fernandez, M. L. Jimenez, and A. V. Delgado, Use of soft electrodes in capacitive deionization of solutions, Environmental Science & Technology **51**, 5326 (2017).

[19] S. Orozco-Barrera, G. R. Iglesias, Á. V. Delgado, S. García-Larios, and S. Ahualli, Effects of layer-by-layer coating on activated carbon electrodes for capacitive deionization, Physical Chemistry Chemical Physics **25**, 9482 (2023).

[20] F. Gao, W. Shi, R. Dai, and Z. Wang, Effective and selective removal of phosphate from wastewater using guanidinium-functionalized polyelectrolyte-modified electrodes in capacitive deionization, ACS ES&T Water **2**, 237 (2021).

[21] S. Sahin, J. E. Dykstra, H. Zuilhof, R. L. Zornitta, and L. C. de Smet, Modification of cation-exchange membranes with polyelectrolyte multilayers to tune ion selectivity in capacitive deionization, ACS applied materials & interfaces **12**, 34746 (2020).

[22] L. Wang, Y. Liang, and L. Zhang, Enhancing performance of capacitive deionization with polyelectrolyte-infiltrated electrodes: theory and experimental validation, Environmental Science & Technology **54**, 5874 (2020).

[23] I. Rubinstein, *Electro-diffusion of ions* (SIAM, 1990).

[24] P. Vanysek, Ionic conductivity and diffusion at infinite dilution, CRC hand book of chemistry and physics , 5 (1993).

[25] R. Zhao, P. Biesheuvel, and A. Van der Wal, Energy consumption and constant current operation in membrane capacitive deionization, Energy & Environmental Science **5**, 9520 (2012).

[26] M. E. Suss, P. Biesheuvel, T. F. Baumann, M. Stadermann, and J. G. Santiago, In situ spatially and temporally resolved measurements of salt concentration between charging porous electrodes for desalination by capacitive deionization, Environmental science & technology **48**, 2008 (2014).

[27] R. J. LeVeque, *Finite Difference Methods for Ordinary and Partial Differential Equations* (SIAM, 2007).

[28] S. Porada, M. Bryjak, A. Van Der Wal, and P. Biesheuvel, Effect of electrode thickness variation on operation of capacitive deionization, Electrochimica Acta **75**, 148 (2012).

[29] C. Lian, M. Janssen, H. Liu, and R. van Roij, Blessing and curse: How a supercapacitor's large capacitance causes its slow charging, Physical Review Letters **124**, 076001 (2020).